Cerium-doped scintillating fused-silica fibers

Published by IOP Publishing for Sissa Medialab

Received: *January 2, 2018*
Accepted: *March 22, 2018*
Published: *April 6, 2018*

2018 JINST 13 P04010

Cerium-doped scintillating fused-silica fibers

N. Akchurin,[1] **C. Cowden, J. Damgov, C. Dragoiu, P. Dudero, J. Faulkner and S. Kunori**

Department of Physics and Astronomy, Texas Tech University,
Lubbock, 79409, TX, U.S.A.

E-mail: nural.akchurin@ttu.edu

Abstract: We report on a set of measurements made on (scintillating) cerium-doped fused-silica fibers using high-energy particle beams. These fibers were uniformly embedded in a copper absorber in order to utilize electromagnetic showers as a source of charged particles for generating signals. This new type of cerium-doped fiber potentially offers myriad new applications in calorimeters in high-energy physics, tracking systems, and beam monitoring detectors for future applications. The light yield, pulse shape, attenuation length, and light propagation speeds are given and discussed. Possible future applications are also explored.

Keywords: Calorimeters; Cherenkov detectors; Scintillators and scintillating fibres and light guides; Timing detectors

[1]Corresponding author.

https://doi.org/10.1088/1748-0221/13/04/P04010

Contents

2018 JINST 13 P04010

1 Introduction

The scintillators for detection of charged particles are common materials in high-energy and nuclear physics experiments. Although these ubiquitous materials are extremely useful and versatile, they suffer degradation when exposed to moderate levels of radiation. Much has been written on the possible damage mechanisms of organic and inorganic scintillators, but a truly radiation-hard scintillator remains elusive today.

In an attempt to develop radiation-hard scintillating and wavelength shifting fibers, we took radiation-hard fused-silica as the base material and doped it with cerium for scintillation as an exploratory step [1]. In this paper, we summarize the outcome of this first step and describe our findings from the first two Ce-doped prototype fibers. These fibers were not optimized for radiation hardness; the radiation hardness studies with more recent fiber productions are ongoing. Here, we report on the basic properties of these types of fibers, discuss future R&D directions, and highlight possibilities afforded with doped-silica optical fibers for instrumentation in particle physics.

2 Experimental setup

2.1 Description of cerium-doped and clear fused-silica fibers

Two types of cerium-doped (denoted as $S^{(1)}$ and $S^{(2)}$) scintillating fibers and Cherenkov radiating (Q) clear fused-silica fibers were produced by Polymicro Technologies[1] for the studies described in this paper. The core preform was doped in volume with cerium by a proprietary dissolving method into the glass matrix, and the Ce:Si molar ratio was 10^{-3} for both $S^{(1)}$ and $S^{(2)}$ fibers. The only difference between the $S^{(1)}$ and $S^{(2)}$ fibers was their dimensions. The doped core was surrounded by a clear fused-silica glass layer, followed by a fluorinated hard-polymer cladding and acrylate

[1]Polymicro Technologies is a subsidiary of Molex located in Phoenix, AZ, USA.

Table 1. The dimensions of the core, glass, cladding, and buffer diameters are listed for the scintillating and clear fibers below, including the numerical apertures.

Fiber	Core dia. [μm]	Glass [μm]	Cladding [μm]	Buffer [μm]	NA
$S^{(1)}$	60 ± 7	200 ± 6	230^{+5}_{-10}	350 ± 15	0.37
$S^{(2)}$	150 ± 20	400 ± 10	430 ± 10	550 ± 30	0.37
Q	-	600 ± 10	630^{+5}_{-10}	800 ± 30	0.33

buffer. The Q-fiber was considerably thicker compared to the scintillating fibers, and unlike the scintillating fibers, the core material was clear fused-silica with no dopants. The fiber dimensions are given in table 1.

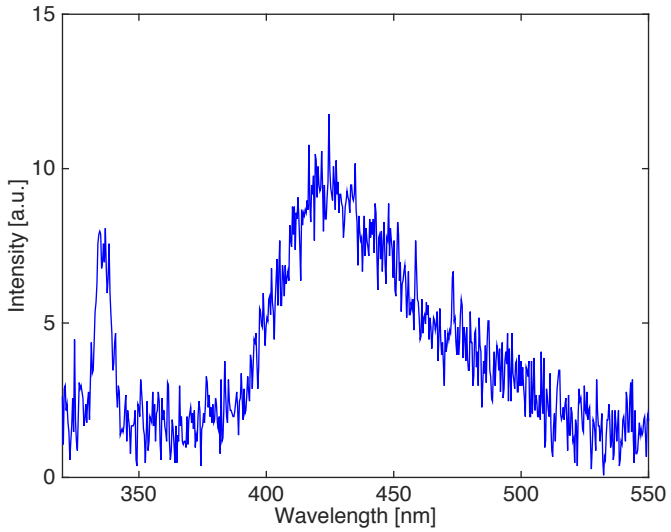

Figure 1. A pulsed nitrogen laser (337 nm) beam was directed axially into a 2-m long $S^{(1)}$-fiber, and the emission spectrum was measured by a spectrometer at the far end. The photoluminescence emission from the cerium-doped core peaks at 430 nm. A small peak corresponding to the laser light at 337 nm is also visible on the left.

Figure 1 shows the emission spectrum of the $S^{(1)}$-fiber when excited by a pulsed N_2 laser. In addition to the photoluminescence peak at 430 nm, a small peak at 337 nm is observed from the nitrogen laser, indicating that some fraction of laser light is transmitted through the glass part of the fiber without interaction.

We also measured the elemental contents of the $S^{(1)}$ and $S^{(2)}$ fibers and compared them to the Q fiber. Table 2 contrasts the concentrations of the measurable elements. We denote the cerium-doped fiber as S because the $S^{(1)}$ and $S^{(2)}$ were drawn from the same core preform and the measurements were consistent. Aside from cerium, the doped-core contained a large amount of Al because it was introduced to inhibit clustering of cerium in the fused-silica matrix. In clear synthetic fused-silica fibers, the aluminum concentration was typically less than 0.04 ppm. The P, Sc, and Zr levels of the fibers are comparable. Along with Ce in the doped-core, we observed sizable concentrations of Ga, Y, La, and Gd.

2018 JINST 13 P04010

Table 2. The element concentrations in the core of scintillating cerium-dope core silica fiber (S) are compared to the clear fused-silica fiber (Q) using laser a ablation inductively-coupled plasma quadrupole mass spectrometer. The units are given in ppm. No quantitative data are provided if the measurement is below detection level.

Fiber	B	Al	P	Sc	Ga	Y	Zr	La	Ce	Gd
S	3	13,000	160	5	160	1	0.2	1.2	5,000	7
Q	6.5	-	95	5	-	-	0.1	-	-	-

Figure 2 shows the arrangement of fibers in a copper structure. The $S^{(1)}$ and Q fibers were embedded in a copper matrix in order to make use of the charged particles in electromagnetic showers as the source of signal in these fibers. The transverse size of the matrix was $4.4 \times 4.4\,\mathrm{cm}^2$, and the length was 200 cm. These dimensions and fiber packing fractions are clearly not ideal for high-energy calorimetry but were dictated by practical concerns, such as sufficient length to measure the optical attenuation lengths of the embedded fibers, adequate mass to contain a reasonable fraction of electromagnetic showers, and reasons of cost. The properties of the Q fibers have been well-studied [2, 3], and the fibers were included in the structure to serve as a basis of comparison. By volume, the matrix consists of the following: 71.72% copper, 20.19% air, 3.53% Q fibers (core only), 0.035% cerium-doped core (denoted as $S_S^{(1)}$) of the $S^{(1)}$-fibers, and 0.357% glass layer of the cerium-doped fiber (denoted as $S_Q^{(1)}$) to signify the Cherenkov component in the $S^{(1)}$-fibers.

The majority of data sets were collected using positrons at 4, 8, 16, and 32 GeV at the MTest beam line at Fermilab. The positrons were identified by a threshold Cherenkov counter in the beam line, and the trigger was formed by two overlapping scintillation counters ($1 \times 1\,\mathrm{cm}^2$) and by the signal from the Cherenkov threshold counter. At lower beam momenta, positrons made up the larger fraction (> 90%) of beam particles.

The main component of the data acquisition is the CAEN domino-ring sampler (DRS) V1742 system. The pulse shapes were sampled at 5 GHz and recorded. Figure 3 shows a collection of pulses from the Q and $S^{(1)}$ PMTs. The pulses from scintillating counters were also digitized by the DRS system, and these pulses were later used to remove the trigger fluctuations event-by-event.

In order to avoid the channelling of beam particles through the holes of the copper matrix, the matrix was tilted by $\theta_V = 2^\circ$ in the vertical plane. It was also set at various angles on the horizontal plane, θ_H, depending on the objectives of the measurement (see figure 2).

3 Results

3.1 The pulse shapes

The light signal from the $S^{(1)}$ fibers is an admixture of Cherenkov and scintillation photons. As noted earlier, we denote the scintillation signal from the doped core as $S_S^{(1)}$ and the Cherenkov signal that comes from the thick glass layer surrounding the core as $S_Q^{(1)}$. While the emission of scintillation photons from the doped fiber core is isotropic, the capture of Cherenkov photons in the fiber depends on the orientation of the fiber axis with respect to the path of the charged particle.

2018 JINST 13 P04010

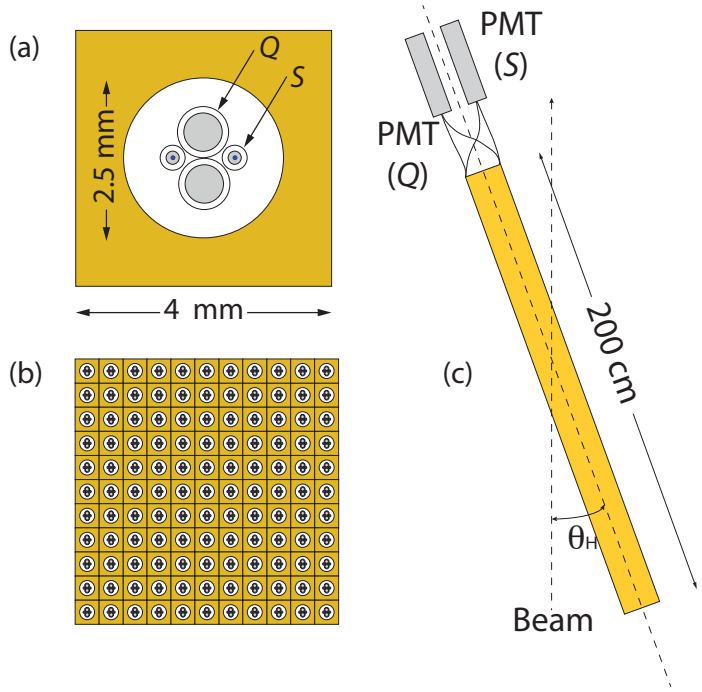

Figure 2. (a) Four fibers -two cerium-doped ($S^{(1)}$) and two clear fused-silica (Q) fibers- were inserted into a single 2.5 mm diameter hole of an extruded ($4 \times 4\,\mathrm{mm}^2$) square copper rod. (b) One hundred and twenty-one of these 200-cm long rods were assembled together, as the transverse cross section shows, to form sufficient mass to contain a sizable fraction of electromagnetic showers when exposed to high-energy electrons. (c) The $S^{(1)}$ and Q fibers were bundled separately and routed to individual PMTs (10-stage Hamamatsu R6427 tubes with 1-1/8-inch-diameter borosilicate glass windows with bialkali photocathode).

If the direction of the Cherenkov photon, emitted at the Cherenkov angle θ_C with respect to the direction of the charged particle is within the numerical aperture (NA) of the fiber, the photon is likely to emerge at the end of the fiber through total internal reflection. If it is not, the photon is lost. In the case of the scintillation light, the entire numerical aperture of the fiber is filled with isotropic light. We took advantage of the directional properties of the Cherenkov radiation and placed the matrix at $\theta_H = 182°$, positioning the PMTs at the upstream end of the setup, thereby minimizing the Cherenkov photon detection efficiency. In this configuration, the average pulse shape from the $S^{(1)}$-fibers is shown in figure 4(a) by a red line. The Cherenkov component ($S_Q^{(1)}$) of the signal was measured using a bandpass filter (UG01-G0401 Melles-Griot), which transmitted the Cherenkov photons between 300 and 400 nm, as shown by a blue line. Because there was no significant scintillation light below 400 nm (see figure 1), this filter was effective in isolating the Cherenkov signal alone. The signal is corrected for the average filter transmission efficiency in figure 4.

The tail of the scintillation pulse is modeled by a sum of two exponential functions: $S_S^{(1)}(t) = a_1 \exp(-t/\tau_1) + a_2 \exp(-t/\tau_2)$, where a_1 and a_2 characterize the relative contribution of the two components, and τ_1 and τ_2, the two characteristic decay times. The fit to the tail (black line) results in $\tau_1 = 20.8 \pm 5.4$ and $\tau_2 = 93.0 \pm 12.6$ ns. The fractional contributions of these components to the scintillation light are $23.9 \pm 5.3\%$ and $76.1 \pm 5.3\%$, respectively, when the pulse is considered within a 200-ns window. The gray shaded area in figure 4 represents the sum, $S_S^{(1)} + S_Q^{(1)}$.

2018 JINST 13 P04010

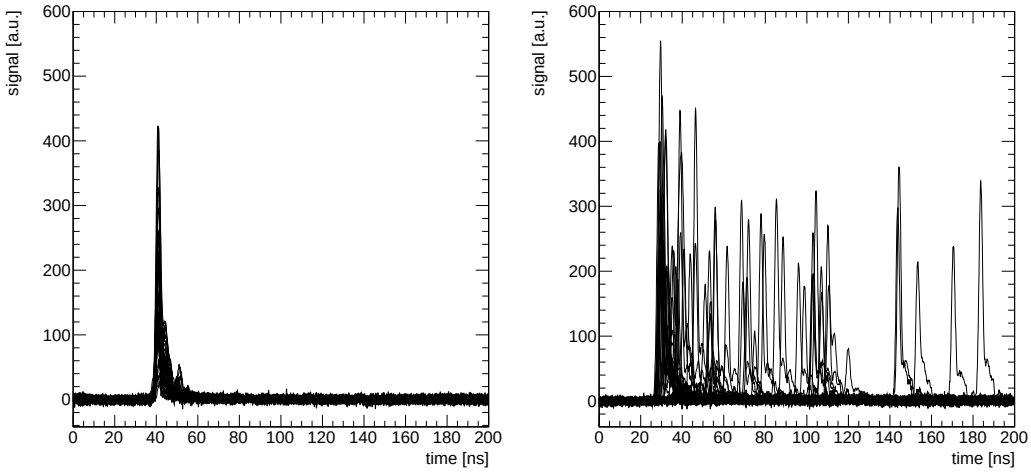

(a) (b)

Figure 3. Fourty individual pulses from (a) clear fused-silica and (b) $S^{(1)}$ fiber bundles are shown when the matrix was exposed to 16 GeV positrons at $\theta_H = 182°$. The Cherenkov light produces prompt and fast pulses, whereas the scintillation photons appear at different times, dictated by the decay life times of the excited states. It is also worth noting that most individual pulses correspond to single photoelectrons.

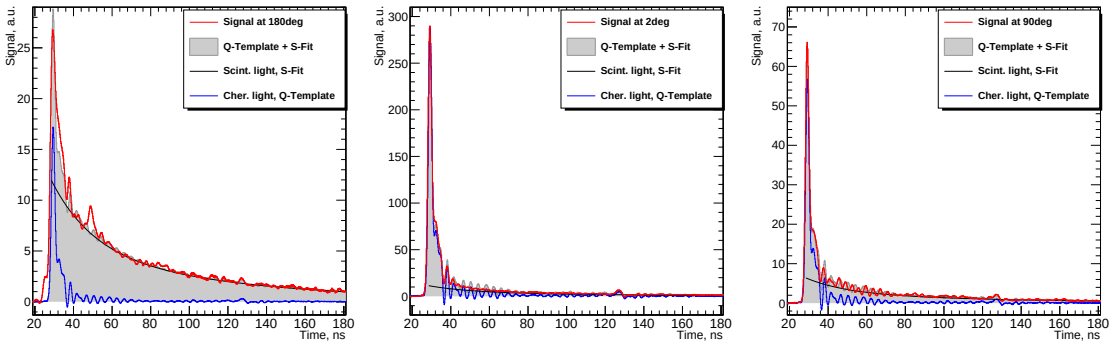

(a) (b) (c)

Figure 4. The *S*-fiber signal shape is formed by a mixture of scintillation and Cherenkov photons in different times of the pulse formation. The scintillation component is modeled by an analytic function (black line), and the Cherenkov part (blue line) is extracted by the use of a bandpass filter. See text for details.

The decay times of cerium-doped fused-silica (SiO_2:Ce^{+3}) ingots produced by the sol-gel technique were reported by Vedda et al. [4]. Depending on the thermal treatment of the ingots and the cerium concentration, they found somewhat different decay times and fractional contributions of these transitions to the total signal. For the Ce:Si molar ratio of 10^{-3} and after rapid thermal treatment (RTT), they reported $\tau_1 = 32 \pm 10$ ns and $\tau_2 = 80 \pm 8$ ns with fractional contributions of 23% and 77% to the total signal, respectively, when the pulse shape was modeled in the same way as in our analysis. If the glass densification was performed at 1050°C without RTT, $\tau_1 = 5 \pm 3$ and $\tau_2 = 74 \pm 6$ ns with relative contributions of 11% and 98%, respectively. Our results are in fair

2018 JINST 13 P04010

agreement with their findings, and the differences likely stem from the doping method (sol-gel *vs.* dissolving) and the thermal history of the samples (ingot samples *vs.* optical fibers).

As can be deduced from figure 4, at $\theta_H = 182°$, the Cherenkov light contributes 14% of the signal in the $S^{(1)}$-fiber. The level of contribution increases to 40% at 90° and to 67% at 2°. It is important to note that the amount of cerium-doped core that is responsible for the scintillation light is only one tenth of the glass layer by volume. Depending on the application, the thickness of the glass layer can be optimized.

3.2 The light yield

The scintillation light yield for fibers $S^{(1)}$ and $S^{(2)}$ is evaluated by measuring the light signals and comparing them to the GEANT4 simulations. We used a dedicated setup for this measurement: a small bundle of $S^{(1)}$, $S^{(2)}$, or Q fibers was placed between thick absorber plates and positioned close to the electromagnetic shower maximum, at 90 degrees with respect to the 16 GeV electron beam direction.

We took advantage of the temporal features of the pulse shape to estimate the scintillation light yield (see section 3.1) where the scintillation light is modeled as a combination of a delta function, representing the rising edge, and a two-component exponential tail, representing the two different decay times. The Cherenkov signal was modeled by a data-driven template that accounts for all instrumental effects (e.g. the PMT response, electronic time constants, and noise). Using the beam data, we evaluated both types of signal in units of photoelectrons and compared the measured scintillator-to-Cherenkov ratio to that which is obtained from the GEANT4 simulation.

The GEANT4 setup included detailed description of the geometry, fiber bundles, fiber geometry, fiber materials, emission spectrum, and absorber plates. The attenuation properties of the fiber (as presented in section 3.3) and the quantum efficiency of the PMT as a function of the wavelength were also implemented. The production of Cherenkov light was handled by GEANT4. The scintillation light production was implemented as isotropic and proportional to the ionization losses in the Ce-doped core by the charged particles in the electromagnetic shower. The capture of the photons within the fiber and propagation of photons to the PMT were simulated in detail by GEANT4. By tuning the photon yield for energy deposited in the cerium-doped core, we were able to calculate the absolute light yield.

Dominant systematic errors stemmed from the Ce-doped core volume (27%) and differences in the PMT quantum efficiency for the scintillation and Cherenkov photons (15%). The aforesaid scintillation-to-Cherenkov ratio tends to cancel systematic errors due to beam and bundle alignment, optical coupling of bundles to the PMT, and uncertainty in the single photoelectron signal definition in the measurement. We found 460 ± 140 photons/MeV for $S^{(1)}$ and 690 ± 220 photons/MeV for $S^{(2)}$.

3.3 The speed of light propagation and light attenuation length

The speeds of light propagation in the $S^{(1)}$ and Q fibers were measured to be 19.40 ± 0.38 cm/ns and 19.50 ± 0.38 cm/ns, respectively. Not surprisingly, the two propagation speeds are essentially the same within the precision of the measurements as we did not attempt to separate the Cherenkov and/or scintillation photons before they were detected by the PMT. At $\theta_H = 90°$, 40% of the light is due to Cherenkov radiation, and some fraction of this light travels without being absorbed or

2018 JINST 13 P04010

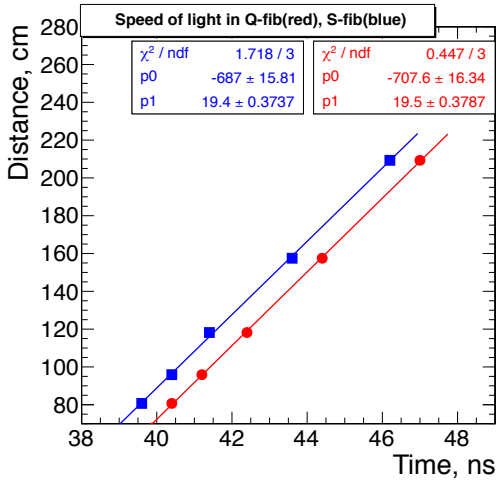

Figure 5. The speed of light propagation was measured in the Q- (red circles) and the $S^{(1)}$- (blue squares) fibers. The fibers were positioned perpendicularly to the beam direction ($\theta_H = 90°$) for this measurement. Each data point represents the time difference between the time of trigger and the arrival of the signal (time-over-threshold) at the PMT as a function of five impact points along the length of the fibers.

wavelength shifted, most likely through the thick glass layer, and is detected by the PMTs. These measurements are consistent with the previously reported values [5, 6] for clear fused-silica fibers used in Cherenkov calorimeters.

Figure 6 shows that when a single exponential function of the form $S^{(1)}(x) = S_0^{(1)} \exp(-x/\lambda_{S^{(1)}})$ and $Q(x) = Q_0 \exp(-x/\lambda_Q)$ is used to describe the measured light attenuation along the fibers, we find $\lambda_Q = 7.4 \pm 0.5$ and $\lambda_{S^{(1)}} = 5.8 \pm 0.7$ m. These values suggest that these fibers, for example, can be used in hadronic calorimeter applications as the light attenuation length is many times longer than typical interaction lengths (~ 20 cm).

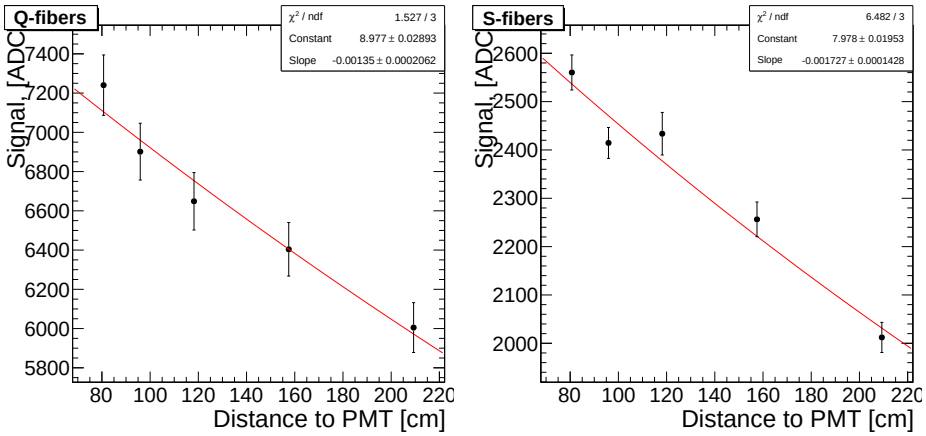

Figure 6. The attenuation length measurements of the Q- (left) and $S^{(1)}$- (right) fibers were carried out by positioning the copper matrix perpendicularly to the direction of beam particles ($\theta_H = 90°$) at five different spots along the matrix. Each data point corresponds to integrated signal within 200 ns as a function of five impact points along the length of the fibers.

2018 JINST 13 P04010

4 Discussion

The need for radiation-hard scintillators beyond what is available today is the primary reason to explore the type of hybrid fiber (the *S*-fiber) described in this paper. The clear fused-silica fibers, because of their superior radiation-hardness, are good candidates to host scintillating dyes. The choice of cerium as a starting point was based on its apparent high light yield, peak emission wavelength appropriate for bialkali PMTs, and potential radiation hardness [7–11]. As much as twice the light yield compared to the $Bi_3Ge_4O_{12}$ (BGO) [12] and tolerance to ~100 kGy in some cerium-doped ingots were reported [4]. Other rare earth materials can also be used as dyes. Praseodymium, for example, is faster (~20 ns), with an emission peak at shorter wavelength (308 nm) compared to cerium [13, 14]. Both the emission spectrum and decay times may be modified by the introduction of co-dopants.

Silica fibers doped in this way offer another interesting feature: they do not contain hydrogen. This property may have a useful implication, especially in calorimetry. Event-by-event compensation results in significant performance improvement when plastic scintillating and clear fibers are used in dual-readout calorimetry [15]. Because the clear (Cherenkov) fibers are mainly sensitive to the electromagnetic core of hadronic showers, it is possible to keep track, event-by-event, of the large fluctuation in π^0 production in hadronic showers and to effectively compensate ($e/h = 1$) the energy measurement. If, in addition to plastic scintillating fibers, rare earth doped fibers such as the $S^{(1)}$-fiber are introduced in a triple-readout scheme, then it is possible to track the next largest fluctuation, i.e. the fluctuations originating from binding energy losses in nuclear break-up, by measuring neutrons of a few MeV. In principle, this can be accomplished by measuring the signal difference between the two scintillating (hydrogenous *vs* non-hydrogenous) fibers on an event-by-event basis.

The *S*-fiber is especially well-suited as a wavelength shifting fiber (WLS) in light collection from a CeF_3 crystal. There is substantial overlap between the excitation of the SiO_2:Ce^{+3} and the emission band of the CeF_3. The electromagnetic calorimeter prototypes constructed using this combination crystal with tungsten absorber and WLS perform very well and show better than 10% stochastic term in the energy resolution [16].

Acknowledgments

We thank the test beam operations team at Fermilab's MTest line for helping with logistics during data taking; Jim Clarkin and Teo Tichindelean from Polymicro Technologies for their expertise in all things fiber and speedy production of the *S*-fibers; Francesca Nessi-Tedaldi from ETH-Zurich for her work on CeF_3 crystal calorimeters; and Anna Vedda, Norberto Chiodini, and Tommaso Tabarelli de Fatis from the University of Milan-Bicocca and INFN-Milan for sharing a wealth information on cerium-doped silica and providing valuable feedback during these studies.

References

[1] M. Nikl et al., *Single-Crystal Scintillation Materials*, in *Springer Handbook of Crystal Growth*, G. Dhanaraj, K. Byrappa, V. Prasad and M. Dudley eds., Springer, Berlin Germany (2010), pg. 1663.

[2] G. Bayatian et al., *Design, performance and calibration of the CMS forward calorimeter wedges*, *Eur. Phys. J.* **C 53** (2008) 139.

2018 JINST 13 P04010

[3] K. Cankocak et al., *Radiation-hardness measurements of high OH- content quartz fibres irradiated with 24-GeV protons up to 1.25-Grad*, *Nucl. Instrum. Meth.* **A 585** (2008) 20.

[4] A. Vedda et al., *Insights into Microstructural Features Governing Ce3+ Luminescence Efficiency in Sol-Gel Silica Glasses*, *Chem. Mater.* **18** (2006) 6178.

[5] P. Gorodetzky et al., *Quartz fiber calorimetry*, *Nucl. Instrum. Meth.* **A 361** (1995) 161.

[6] N. Akchurin et al., *Beam test results from a fine-sampling quartz fiber calorimeter for electron, photon and hadron detection*, *Nucl. Instrum. Meth.* **A 399** (1997) 202 [INSPIRE].

[7] A. Vedda et al., *Ce3+-doped fibers for remote radiation dosimetry*, *Appl. Phys. Lett.* **85** (2004) 6356.

[8] I. Veronese et al., *Feasibility study for the use of cerium doped fibers in proton therapy*, *Rad. Meas.* **45** (2010) 635.

[9] N. Caretto et al., *Feasibility of dose assessment in radiological diagnostic equipments using Ce-doped radio-luminescent optical fibers*, *Nucl. Instrum. Meth.* **A 612** (2010) 407.

[10] I. Veronese et al., *Study of the radio luminescence spectra of doped silica optical fibre dosimeters for stem effect removal*, *J. Phys.* **D 46** (2013) 015101.

[11] M. Carrara et al., *Characterization of Ce3+ doped SiO2 optical dosimeter for dose measurements in HDR brachytherapy*, *Rad. Meas.* **56** (2013) 312.

[12] N. Chiodini et al., *High-efficiency SiO2:Ce3+ glass scintillators*, *Appl. Phys. Lett.* **81** (2002) 4374.

[13] J. Pejchal et al., *Pr^{3+}-doped complex oxide single crystal scintillators*, *J. Phys.* **D 42** (2009) 055117.

[14] Y. Sun et al., *Synthesis and characterization of Pr^{3+}-doped glass scintillators prepared by the sol-gel method*, *J. Sol-Gel Sci. Technol.* **62** (2012) 313.

[15] N. Akchurin et al., *Hadron and jet detection with a dual-readout calorimeter*, *Nucl. Instrum. Meth.* **A 537** (2005) 537.

[16] R. Becker et al., *Proof-of-principle of a new geometry for sampling calorimetry using inorganic scintillator plates*, in *Proceedings of CALOR2014, the International Conference on Calorimetry for High Energy Physics*, Giessen Germany (2014), and in *Proceedings of the International Conference on the Technology and Instrumentation in Particle Physics 2017 (TIPP2017)*, Beijing China (2017) [arXiv:1405.6202].

2018 JINST 13 P04010